International Journal of Research and Review
[Indexed, Peer-Reviewed Journal]
Volume 12; Issue: 12; December 2025
Website: www.ijrrjournal.com
Research Paper *E-ISSN: 2349-9788; P-ISSN: 2454-2237*

Dose Reduction Potential in Pediatric Chest CT: Comparative Analysis of Tube Voltage and Patient Protocol Presets Using a Custom Pediatric Chest Phantom

Muhammad Ghulam Raihan[1], Jatmiko Endro Suseno[1], Asep Yoyo Wardaya[1], Heri Sutanto[1]

[1]Department of Physics, Faculty of Sciences and Mathematics, Diponegoro University, Semarang 50275, Indonesia

Corresponding Author: Muhammad Ghulam Raihan

DOI: https://doi.org/10.52403/ijrr.20251285

ABSTRACT

Computed Tomography (CT) contributes significantly to medical radiation exposure, demanding rigorous dose optimization, especially for the radiosensitive pediatric population, yet high dose variability often results from inappropriate protocol selection. To address this, a custom-developed pediatric chest phantom, radiologically representative of a 7-year-old child, was utilized to systematically quantify dose impacts. The phantom was scanned using a Toshiba Aquilion Prime CT scanner across two protocol presets (adult chest and pediatric chest) at three tube voltage settings (80, 100, and 120 kV), with the pediatric protocol engaging the Automated Exposure Control (AEC). Dose metrics, including Volume CT Dose Index (CTDIvol) and Size-Specific Dose Estimate (SSDE), were calculated via the validated IndoseCT platform. The results demonstrated that the adult protocol consistently yielded SSDE values that were approximately 3.0 to 3.4 times greater than the pediatric protocol across all kV levels. Specifically, raising the tube voltage in the adult protocol caused a sharp rise in SSDE (from 2.10 mGy at 80 kV to 5.81 mGy at 120 kV). In contrast, the pediatric protocol maintained a highly stable SSDE (ranging from 1.52 mGy to 1.73 mGy) due to effective AEC compensation. In conclusion, the use of inappropriate adult presets for pediatric CT introduces a substantial and avoidable radiation dose penalty, potentially leading to doses that exceed established Diagnostic Reference Levels (DRLs). This study reinforces the critical necessity of strict adherence to size- and age-specific protocols and optimal AEC engagement as the primary strategy for achieving significant dose reduction in pediatric CT imaging.

Keywords: Pediatric CT, Dose Reduction, SSDE, Tube Voltage, Protocol Optimization, Pediatric Phantom

INTRODUCTION

Computed tomography (CT) contributes substantially to global medical radiation exposure. Although CT accounts for only about 25% of imaging procedures, it delivers up to 78% of the total medical radiation dose. Approximately 10% of CT examinations are performed in pediatric patients, whose smaller body size and higher tissue radiosensitivity increase lifetime attributable risks (1). Therefore,

ensuring optimized radiation dose while preserving diagnostic quality is essential, particularly under the ALARA principle (2). Dose variation in pediatric CT remains a major challenge. Differences in patient size, technologist technique, and the common—but inappropriate—use of adult protocol presets can lead to significant dose variations approaching twofold across facilities (3). Furthermore, optimizing technical parameters, particularly tube voltage (kV), is crucial for dose reduction without compromising diagnostic quality. Low-dose chest CT is increasingly used, yet protocol standardization continues to be inconsistent (4).

To support optimization, several tools have been developed to estimate radiation dose using DICOM metadata. IndoseCT is among the most validated platforms, capable of automatically calculating water-equivalent diameter (Dw), size-specific dose estimate (SSDE), and organ dose (5). Its accuracy has been confirmed to be within ±10% compared with ion chamber measurements (6).

Because direct organ-dose measurement in pediatric patients is impractical and ethically restricted, phantoms are essential for controlled CT dose studies (7). While standard phantoms exist, anthropomorphic phantoms provide more realistic anatomy and attenuative properties crucial for pediatric dosimetry (8). However, commercial anthropomorphic phantoms are often prohibitively expensive (9,10). This gap necessitates the development of cost-effective, regionally accessible phantoms that accurately mimic pediatric anatomy, providing a reliable platform to evaluate and optimize clinical CT protocols.

Given the high radiation contribution from CT, the sensitivity of pediatric patients, and the recognized inconsistency in protocol selection, a systematic study is warranted. Previous studies have attempted custom phantom development but often lacked the specific focus on quantifying the dose impact of current clinical protocol presets (adult vs. pediatric) across varying kV levels. Therefore, this study aims to comparatively analyze the dose reduction potential in pediatric chest CT. Specifically, we quantify and compare the Size-Specific Dose Estimate (SSDE), CTDIvol, and DLP derived from IndoseCT, as a function of varying tube voltages (kV) and the selection of adult versus pediatric protocol presets using a custom pediatric chest phantom. The results are expected to contribute significantly to evidence-based optimization strategies for pediatric chest CT examinations.

MATERIALS & METHODS

Fabrication of Pediatric Phantom

The pediatric lung phantom represents the thoracic anatomy of a 7-year-old child. The model was constructed from ten layers of 10 mm PMMA sheets, resulting in final dimensions of 230 x 158 mm with an axial thickness of 100 mm. The geometric contour was derived from pediatric chest CT data to approximate realistic thoracic morphology for dose evaluation, consistent with prior approaches for developing age-specific phantoms (11,12). Each PMMA layer was cut using a laser-cutting machine following the segmented thoracic contour. The internal cavities were then filled with tissue-equivalent substitute materials: a resin–calcium carbonate mixture for bone-equivalent structures, PMMA regions for soft tissue equivalence, and Polyurethane (PU) foam as a lung-equivalent material. These materials were selected due to their radiological properties—particularly density and Hounsfield Unit (HU) similarity—based on previous phantom development studies (2,12–14). The final phantom was assembled layer-by-layer to create a stable axial model suitable for CT dosimetric evaluation. The detailed fabrication process is provided in Figure 1. To ensure the material's suitability, the Hounsfield Unit (HU) linearity was verified by measuring the mean HU of the central region of interest (ROI) for each material on a 120 kV scan and comparing it with literature values for 7-year-old chest tissue.

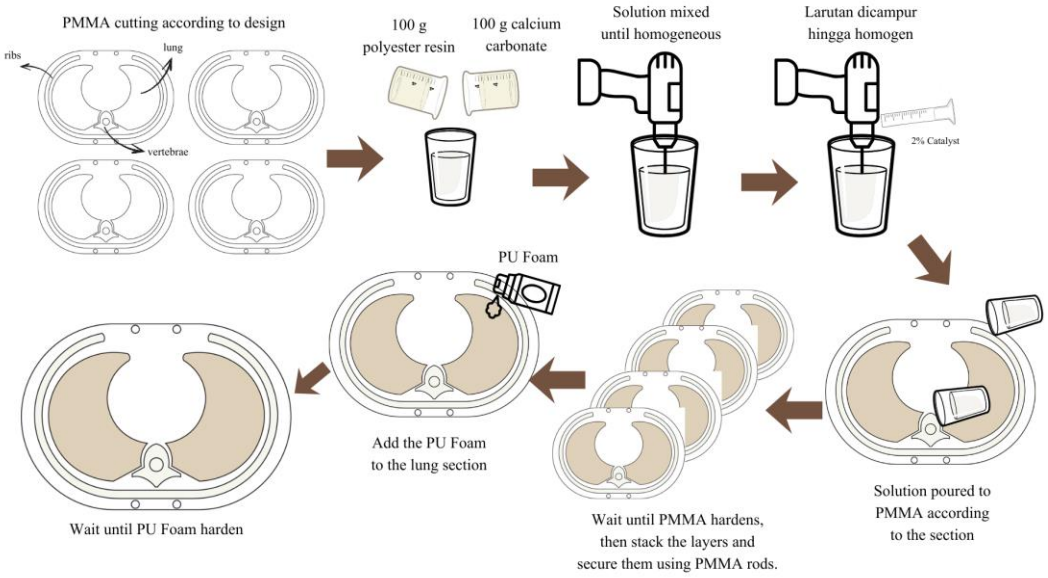

Figure 1. Phantom Fabrication Process

CT Scanner and Protocols

Scanning was performed using a Toshiba Aquilion Prime CT scanner operating in Helical mode. Two types of chest scan presets—adult chest and pediatric chest—were applied across three tube-voltage settings (80, 100, and 120 kV). All scans utilized the Automatic Exposure Control (AEC) system of the scanner, specifically setting the Quality Reference mAs (QRM) for each protocol to the values specified in Table 1. The primary differences between the two clinical presets were slice thickness (5 mm vs 2 mm), rotation time (0.35 s vs 0.5 s), and the baseline QRM, reflecting standard clinical distinctions between adult and pediatric CT dose-optimization strategies.

Dose Calculation Using IndoseCT

Dose indices were calculated using IndoseCT, a validated platform that extracts and computes dose metrics directly from DICOM metadata. The calculated metrics included the Size-Specific Dose Estimate (SSDE), Water-Equivalent Diameter (D_W), Volume Computed Tomography Dose Index ($CTDI_{vol}$), and Effective Dose (E). IndoseCT computes SSDE based on the American Association of Physicists in Medicine (AAPM) Report 204 methods using D_W extracted from DICOM images. The Effective Dose (E) was calculated from the organ doses determined by IndoseCT, applying the tissue weighting factors (ω_T) as established in ICRP Publication 103 for consistency and clinical relevance (5). Dose analysis was performed descriptively to observe trends across varying tube voltage and protocol presets.

Table 1. CT Chest Protocol Parameters

Protocol	Tube Voltage (kV)	Tube Current (mA)	Slice Thickness (mm)	Rotation Time (s)	Pitch
Adult	80	97	5	0.35	0.813
Adult	100	80	5	0.35	0.813
Adult	120	80	5	0.35	0.813
Pediatric	80	80	2	0.5	0.813
Pediatric	100	40	2	0.5	0.813
Pediatric	120	25	2	0.5	0.813

RESULT

Phantom Characterization and CT Number Validation

Figure 2. Physical Characteristic of the Phantom

A custom pediatric lung phantom was fabricated based on the axial thoracic anatomy of a 7-year-old child, with final dimensions of 230 x 158 mm and a total height of 100 mm. The phantom, constructed from 10 stacked PMMA layers, included structures equivalent to bone (resin–calcium carbonate), soft tissue (PMMA regions), and lung parenchyma (PU foam). The physical characteristics of the phantom are depicted in Figure 2. The CT Number values measured from the central regions of interest (ROI) of each tissue-equivalent material, scanned at 100 kV, are presented in Table 2, alongside patient reference values. The reference CT number value obtained from (15,16). The measured CT numbers for the PMMA and the resin–calcium carbonate mixture fell within the established ranges for soft tissue and bone, respectively. Specifically, the soft tissue-equivalent PMMA measured 98 HU and the resin–calcium carbonate measured 896 HU, which aligns closely with reported pediatric bone density values. The CT number for the lung-equivalent PU foam was measured at -954 HU.

Table 2. CT Number on images of patient and phantom

Tissue	Reference CT Number (HU)	Measured CT number on patient image (HU)	Measured CT number on the pediatric chest phantom (HU)
Soft Tissue	-700 to 225	68 ± 14	98
Bone	568 to 2198	805 ± 244	896
Lung	-950 to -600	-656 ± 66	-954

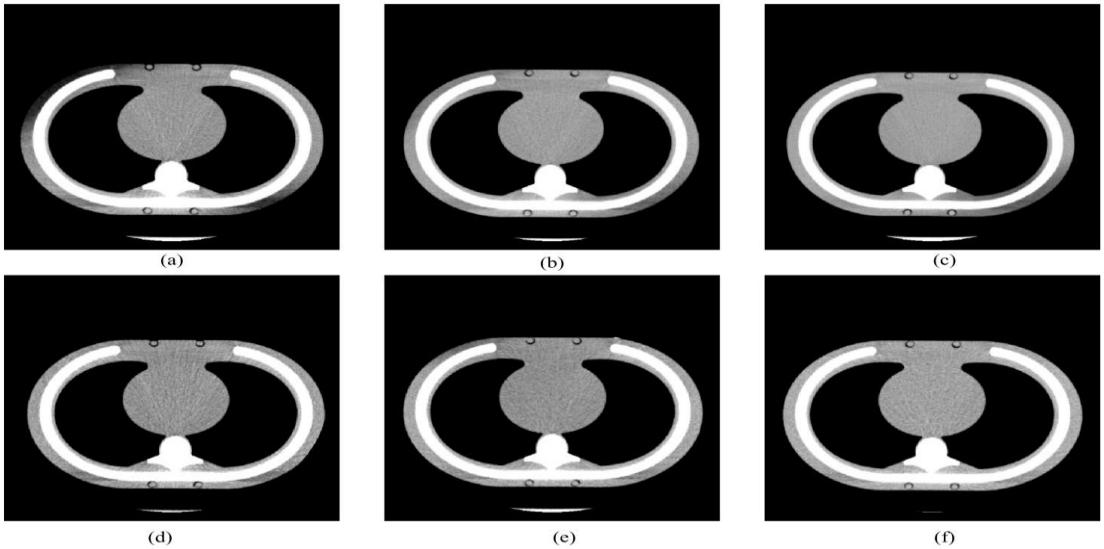

Figure 3. Axial CT images of the custom pediatric chest phantom showing the comparison between Adult and Pediatric protocol presets at varying tube voltages. Top row (Adult Protocol): (a) 80 kV, (b) 100 kV, and (c) 120 kV. Bottom row (Pediatric Protocol): (d) 80 kV, (e) 100 kV, and (f) 120 kV.

CT Image Analysis

Figure 3 presents the CT axial images of the phantom obtained at 80, 100, and 120 kV using both adult and pediatric protocols. Visually, an increase in tube voltage was associated with a decrease in image contrast

across both protocol types. Furthermore, qualitative observation indicated that the adult protocol generally produced lower image noise across all tube voltage settings compared to the corresponding pediatric protocol settings. This noise difference was most notable in the lung and soft tissue regions. Differences between the two protocols also indicate that the adult protocol produces lower noise, which aligns with the inverse relationship between noise and the square root of mAs. Because adult settings use higher mA, noise is expected to be lower (15,17–19).

Dose Measurement Analysis

The dose metrics calculated using IndoseCT for the six different scan conditions are summarized in Table 3. The Water-Equivalent Diameter (D_W) for the phantom, ranging from 17.7 cm to 18.2 cm, was consistent across all scans.

Table 3. Dose metrics measured using IndoseCT

Protocol	Tube Voltage (kV)	Tube Current (mA)	Slice Thickness (mm)	CTDIvol (mGy)	DW (cm)	SSDE (mGy)	Effective Dose (mSv)
Adult	**80**	**97**	5	1,1	18,10	2,1	0,02
Adult	**100**	**80**	5	1,8	17,86	3,46	0,04
Adult	**120**	**80**	5	3	17,68	5,81	0,06
Pediatric	**80**	**80**	2	0,8	18,20	1,52	0,01
Pediatric	**100**	**40**	2	0,8	17,82	1,54	0,01
Pediatric	**120**	**25**	2	0,9	17,85	1,73	0,01

Effect of Tube Voltage on Dose (Adult vs Pediatric Protocol)

For the adult protocol, increasing tube voltage from 80 to 120 kV resulted in substantial increases in CTDIvol from 1.10 to 3.00 mGy and SSDE from 2.10 to 5.81 mGy. In contrast, the pediatric protocol exhibited relatively stable CTDIvol values, with only a minor increase from 0.80 mGy at 80 kV to 0.90 mGy at 120 kV. This stability was reflected in the SSDE values, which remained nearly constant, ranging from 1.52 mGy to 1.73 mGy across the tested kV range as we see in Figure 4 and Figure 5.

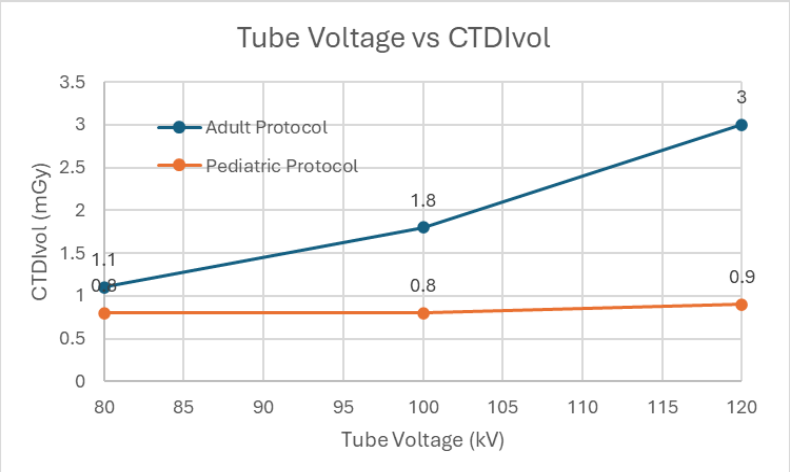

Figure 4. Comparison of Volume CT Dose Index ($CTDI_{vol}$) as a function of Tube Voltage (kV) for Adult and Pediatric protocol presets

Comparative Analysis of Protocol Presets

Across all tested tube voltages, the adult protocol consistently yielded significantly higher SSDE values compared to the pediatric protocol. Specifically, the SSDE values generated by the adult protocol were

approximately 3.0 to 3.4 times greater than the corresponding SSDE values obtained using the pediatric protocol at the same tube voltage. The maximum SSDE recorded was 5.81 mGy at adult presets with 120 kV, which was over three times the maximum SSDE recorded for the pediatric protocol 1.73 mGy at 120 kV.

Similarly, the analysis of Effective Dose (E) revealed the same trend in risk assessment, as shown in Figure 6. For the adult protocol, the effective dose increased substantially from 0.02 mSv at 80 kV to 0.06 mSv at 120 kV. In contrast, the pediatric protocol maintained a very low and stable effective dose of 0.01 mSv across the entire kV range. The highest effective dose measured using the adult protocol (0.06 mSv) was 6 times higher than the highest effective dose measured using the pediatric protocol (0.01 mSv).

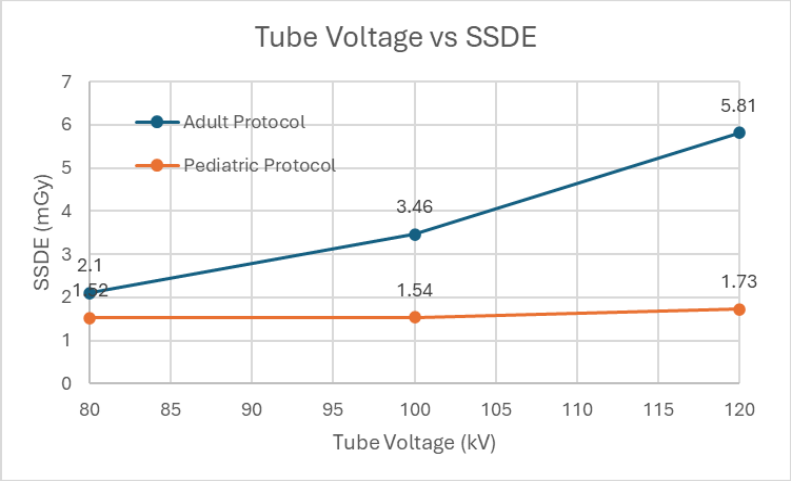

Figure 5. Comparison of Size-Specific Dose Estimate (SSDE) as a function of Tube Voltage (kV) for Adult and Pediatric protocol presets

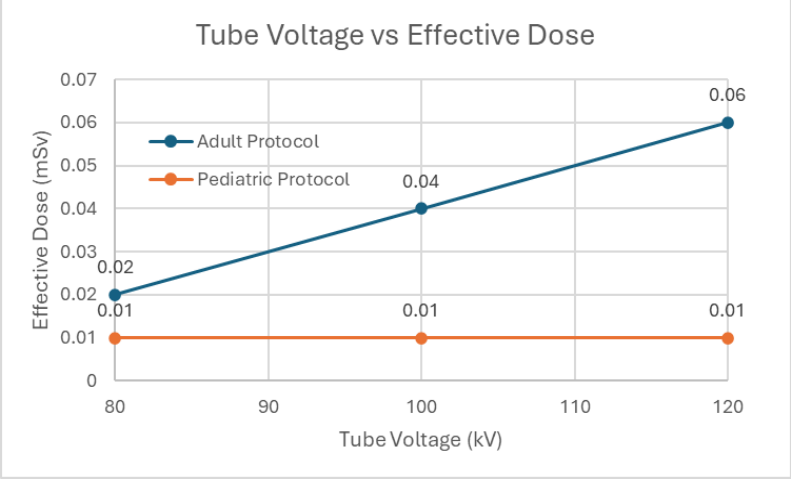

Figure 6. Comparison of Effective Dose (E) as a function of Tube Voltage (kV) for Adult and Pediatric protocol presets

DISCUSSION

This study utilized a phantom fabricated using DICOM data from a 7-year-old patient, employing materials with similar radiological characteristics, thereby aiming for the phantom to represent the patient's physical and radiological properties. As shown in Table 2, the CT number of the soft tissue-equivalent PMMA was higher than the CT number measured in the patient's image. This is attributed to PMMA having a higher electron density, which results in

increased X-ray attenuation, thus leading to a higher CT number (14). This measured value aligns with previous studies (12,14,20). Although the PMMA CT number was higher than the patient's measured value, the PMMA CT number still fell within the accepted range for soft tissue (14–16). The substitute material for bone had a slightly higher CT number than the CT number measured in the patient. This is because this study used calcium carbonate (wt50%). The CT number ranged from 982 ± 7 HU. The CT number of this material can be adjusted by reducing the calcium carbonate content or increasing the polyester resin (13,14). The PU foam used as a substitute material for lung tissue also had a lower CT number compared to the lung tissue measured in the patient. This is consistent with previous studies (2,21). Although the CT number was lower than the patient's CT number, this is because the measurement of the lung soft tissue CT number includes the air and vessels present in the lungs, whereas the PU foam CT number contains only air (2).

The analysis of the dose metrics revealed a significant difference in system behavior between the adult and pediatric protocol presets. For the adult protocol, increasing the tube voltage from 80 kV to 120 kV resulted in a substantial rise in $CTDI_{vol}$ and SSDE. This finding aligns with fundamental X-ray physics, where higher kV increases photon fluence and energy spectrum, subsequently increasing the radiation output and patient dose. SSDE is affected by both values of CTDIvol and size-correction factor. SSDE decreases with size in the head due to constant mA (or fixed tube current, FTC). The constant mA leads to a constant CTDIvol. This constant CTDIvol then results in a decreasing of SSDE, because of the decrease in size-correction factor. Conversely, the other examinations use tube current modulation (TCM) for dose reduction in small patients, where the mA increases with the size. This increase of mA leads to an increase in CTDIvol. If the size increases, the CTDIvol increases but the size-correction factor decreases. The combination of the increase of CTDIvol and a decrease of size correction factor can lead SSDE to remain constant, or increase, or decrease depending on which one is more dominant. This dominance depends on the magnitude of TCM (15,22,23). In sharp contrast, the Pediatric protocol demonstrated remarkable stability in $CTDI_{vol}$ and SSDE across the same kV range. This phenomenon is a direct result of the system's dose-optimization strategy, where the Automated Exposure Control (AEC) system aggressively reduces the Tube Current (Ma/QRM) at higher voltages to maintain a consistent image noise level. This behavior confirms the effective implementation of dose-reduction techniques designed for pediatrics, where the AEC successfully maintains low-dose conditions despite changes in the tube voltage. Furthermore, the lower image noise observed in the adult protocol compared to the pediatric protocol directly reflects the higher mA settings used in the adult presets, which follows the general principle of the inverse relationship between noise and the square root of mAs as we see in Figure 2 (18,22,24).

The most critical finding is the quantified dose difference between the two protocol types. The adult protocol consistently yielded SSDE values that were approximately three to four times higher than those generated by the pediatric protocol, even when scanning the identical phantom at the same tube voltage. This significant variation underscores the substantial radiation penalty incurred when an inappropriate adult preset is utilized for a pediatric patient (3). By focusing on the SSDE, which is the most relevant metric for size-specific patient dose estimation as it accounts for patient size, our data reinforce the importance of tailored protocols (25).

The maximum SSDE recorded using the adult 120 kV protocol (5.81 mGy) substantially exceeds the doses obtained with the pediatric optimized settings (1.73 mGy). This disparity is further highlighted

by the Effective Dose (E) assessment (Figure 6). The Effective Dose for the adult protocol increased sharply from 0.02 mSv to 0.06 mSv, while the pediatric protocol maintained a constant low dose of 0.01 mSv. This means the highest effective dose measured using the adult protocol was six times (6x) higher than the maximum dose from the pediatric protocol, signifying a major difference in radiation risk. When compared to international benchmarks, this high dose level likely exceeds established Diagnostic Reference Levels (DRLs) for 6-to8-year-old chest CT (26) highlighting a major optimization failure in clinical practice when protocol selection is not strictly age- and size-appropriate. The stability of the SSDE and E in the pediatric protocol suggests that optimization efforts should focus on ensuring the proper selection and activation of pediatric AEC presets, rather than solely on manual kV adjustments, to maintain the lowest possible dose.

This study has several limitations, primarily related to the scope of the equipment and phantom used. Firstly, only one type of phantom and one type of scanner were utilized. Therefore, further studies involving different phantom types and various CT scanners are necessary to fully generalize the observed dose reduction effects between the adult and pediatric chest protocols. Secondly, the values of Signal-to-Noise Ratio (SNR) and Contrast-to-Noise Ratio (CNR) were not calculated. These image quality metrics are crucial and should be calculated in future research to fully understand the effects of tube voltage, tube current, and AEC on image quality. Furthermore, this study relied solely on IndoseCT software for dose estimation. Although previous research has shown that the difference in SSDE between IndoseCT and direct measurement is only ± (6), direct dose measurement using dose probes within the materials used to construct the phantom is still required to provide a robust comparison.

CONCLUSION

This comparative dosimetric analysis utilizing a custom pediatric chest phantom provides strong evidence regarding the critical impact of protocol selection and tube voltage on CT radiation dose. The study decisively found that the use of non-optimized adult protocol presets consistently resulted in Size-Specific Dose Estimate (SSDE) values that were 3.0 to 3.4 times higher than those generated by the optimized pediatric protocol. This significant, avoidable dose penalty indicates that adult protocols pose a substantial risk of exceeding established Diagnostic Reference Levels (DRLs) for pediatric patients. Conversely, the pediatric protocol demonstrated remarkable dose stability across varying tube voltages (80 kV to 120 kV), confirming the high effectiveness of the Automatic Exposure Control (AEC) system when properly optimized for pediatric settings. Therefore, this research concludes that the primary strategy for achieving maximal dose reduction in pediatric chest CT lies in the strict adherence to size- and age-specific protocol selection and ensuring optimal function of the AEC system, rather than relying solely on manual tube voltages adjustments.

Declaration by Authors

Acknowledgement: None
Source of Funding: None
Conflict of Interest: No conflicts of interest declared.

REFERENCES

1. Sulieman A, Almogren KS, Tamam N. Radiation exposure estimation in pediatric patients during computed tomography imaging procedures. Radiation Physics and Chemistry. 2023; 204:110653. DOI: 10.1016/j.radphyschem.2022.110653
2. Pengpan T, Rattanarungruangchai N, Dechjaithat, et al. Optimization of Image Quality and Organ Absorbed Dose for Pediatric Chest X-Ray Examination: In-House Developed Chest Phantom Study. Radiology Research and Practice. 2022; 2022:1–10. DOI: 10.1155/2022/3482458

3. Almujally A, Tamam N, Sulieman A, et al. Evaluation of paediatric computed tomography imaging for brain, and abdomen procedures. Radiation Physics and Chemistry. 2022; 200:110271. DOI: 10.1016/j.radphyschem.2022.110271
4. Miftahuddin D, Prayitno AG, Hariyanto AP, et al. Evaluation of low-dose pediatric chest CT examination using in-house developed various age-size pediatric chest phantoms. European Journal of Radiology. 2024; 177:111599. DOI: 10.1016/j.ejrad.2024.111599
5. Anam C, Fujibuchi T, Han D, et al. Estimated organ dose using the size-specific dose estimates (SSDE) and its comparison with direct measurements. Radiation Measurements. 2025; 189:107515. DOI: 10.1016/j.radmeas.2025.107515
6. Dio P, Anam C, Hidayanto E, et al. Evaluation of radiation dose accuracy calculated using IndoseCT software with direct measurement on polyester-resin phantoms. Radiation Physics and Chemistry. 2022; 201:110473. DOI: 10.1016/j.radphyschem.2022.110473
7. Pandiangan T, Bali I. Analisis Dosis Radiasi Pada Jaringan Tumor Dengan Simulasi Program Mcnp-5. Jurnal Muara Sains, Teknologi, Kedokteran, dan Ilmu Kesehatan. 2021; 5(2):341. DOI: 10.24912/jmstkik. v5i2.9348
8. Wegner M, Gargioni E, Krause D. Classification of phantoms for medical imaging. In: Liu A, Kara S. 33rd CIRP Design Conference; 2023 May 17-19; Sydney, Australia. Elsevier; 2023. p.1140–1145. DOI: 10.1016/j.procir.2023.03.154
9. Hernandez-Giron I, Den Harder JM, Streekstra GJ, et al. Development of a 3D printed anthropomorphic lung phantom for image quality assessment in CT. Physica Medica. 2019; 57:47–57. DOI: 10.1016/j.ejmp.2018.11.015
10. Mei K, Geagan M, Roshkovan L, et al. Three-dimensional printing of patient-specific lung phantoms for CT imaging: Emulating lung tissue with accurate attenuation profiles and textures. Medical Physics. 2022;49(2):825–35. DOI: 10.1002/mp.15407
11. Jordan P, Adamson P, Bhattbhatt V, et al. Pediatric chest-abdomen-pelvis and abdomen-pelvis CT images with expert organ contours. Medical Physics. 2022; 49(4):2342–2354.
12. Rodgers S, Atkinson J, Cryer D, et al. Construction and validation of an infant chest phantom for paediatric computed tomography. Physical Engineering Sciences in Medicine. 2024; 47(2):491–501. DOI: 10.1007/s13246-023-01379-5
13. Heryani H, Sutanto H, Anam C, et al. Development of Synthetic Bones for ANSI Chest Phantom Dosimetry. European Journal of Engineering and Technology. 2020; 7(9):12-17. Available from: https://ejaet.com/PDF/7-9/EJAET-7-9-12-17.pdf
14. Nisa KA, Anam C, Alkian I, et al. Design and fabrication of paediatric chest phantom using polymethyl methacrylate-polyurethane foam for pneumonia imaging evaluation. Radiation Physics and Chemistry. 2025; 232:112610. DOI: 10.1016/j.radphyschem.2025.112610
15. Dance DR, Christofides S, Maidment ADA, McLean ID, Ng KH. Diagnostic Radiology Physics: A Handbook for Teachers and Students. Vienna: International Atomic Energy Agency (IAEA); 2014. p.280-287. DOI:
16. Chougule VN, Mulay AV, Ahuja BB. Clinical Case Study: Spine Modeling for Minimum Invasive Spine Surgeries (MISS) using Rapid Prototyping. In: IIT Madras Chennai. Proceedings of 10th International Conference on Precision, Meso, Micro, and Nano Engineering (COPEN 10); 2017 Dec 6-9; Chennai, India. IIT Madras Chennai. 2017. p.96-102.
17. Dewi PS, Ratini NN, Trisnawati NLP. Effect of x-ray tube voltage variation to value of contrast to noise ratio (CNR) on computed tomography (CT) Scan at RSUD Bali Mandara. International Journal of Physical Sciences and Engineering. 2022; 6(2):82–90. DOI: 10.53730/ijpse. v6n2.9656
18. Huda W, Abrahams RB. Radiographic Techniques, Contrast, and Noise in X-Ray Imaging. American Journal of Roentgenology. 2015; 204(2): W126–31. Available from: https://ajronline.org/doi/10.2214/AJR.14.13116
19. Satwika LGP, Ratini NN, Iffah M. Pengaruh Variasi Tegangan Tabung Sinar-X terhadap Signal to Noise Ratio (SNR) dengan

Penerapan Anode Heel Effect menggunakan Stepwedge. Buletin Fisika. 2021; 22(1):20. DOI: 10.24843/BF.2021.v22. i01.p04
20. Amini I, Akhlaghi P, Sarbakhsh P. Construction and verification of a physical chest phantom from suitable tissue equivalent materials for computed tomography examinations. Radiation Physics and Chemistry. 2018; 150:51–57. DOI: 10.1016/j.radphyschem.2018.04.020
21. Jamal NHM, Sayed IS, Syed WS. Estimation of organ absorbed dose in pediatric chest X-ray examination: A phantom study. Radiation Physics and Chemistry. 2020; 166:108472. DOI: 10.1016/j.radphyschem.2019.108472
22. Anam C, Budi WS, Adi K, et al. Assessment of patient dose and noise level of clinical CT images: automated measurements. Journal of Radiological Protection. 2019; 39(3):783–793. DOI: 10.1088/1361-6498/ab23cc
23. Bushberg JT, Seibert JA, Leidholdt Jr EM. The essential physics of medical imaging. 3rd ed. Philadelphia: Wolters Kluwer Health/Lippincott Williams & Wilkins; 2012. p.387-400
24. Furukawa Y, Matsubara K, Tsutsumi Y. A comparison of automatic and manual compensation methods for the calculation of tube currents during off-centered patient positioning with a noise-based automatic exposure control system in computed tomography. Physical Engineering Sciences in Medicine. 2021; 44(3):823–832. DOI: 10.1007/s13246-021-01033-y
25. AAPM Task Group 204. AAPM Report No. 204: Size-Specific Dose Estimates (SSDE) in CT. College Park, MD: AIP Publishing, American Institute of Physics (AAPM); 2011. Report No: 204.
26. Rawashdeh M, Saade C, Al Mousa DS, et al. A new approach to dose reference levels in pediatric CT: Age and size-specific dose estimation. Radiation Physics and Chemistry. 2023; 205:110698. DOI: 10.1016/j.radphyschem.2022.110698

How to cite this article: Muhammad Ghulam Raihan, Jatmiko Endro Suseno, Asep Yoyo Wardaya, Heri Sutanto. Dose reduction potential in pediatric chest CT: comparative analysis of tube voltage and patient protocol presets using a custom pediatric chest phantom. *International Journal of Research and Review*. 2025; 12(12): 844-853. DOI: *10.52403/ijrr.20251285*

******